Scattering by Black Holes

Nils Andersson
Department of Mathematics
University of Southampton,
Southampton SO17 1BJ, UK

Bruce Jensen
Department of Mathematics, University of Southampton,
and Marconi Communications,
551-553 Wallisdown Road,
Poole BH12 5AG, UK

This article is a slightly modified version of the authors' contribution to *Scattering*, edited by Roy Pike and Pierre Sabatier, to be published by Academic Press.

I. WHAT IS A BLACK HOLE?

Black holes, objects so compact that not even light can escape their gravitational pull, are among the most intriguing concepts of modern science. As Kip Thorne wrote in 1974: "Of all the conceptions of the human mind from unicorns to gargoyles to the hydrogen bomb perhaps the most fantastic is the black hole: a hole in space with a definite edge over which anything can fall and nothing can escape; a hole that curves space and warps time." Evidence that these exotic objects exist in our universe has been mounting since the discovery of the archetypal black hole Cygnus X1 in 1971. Today, the presence of supramassive black holes (several million times as massive as our sun) at the centre of many galaxies, and smaller black holes (5-10 times as massive as the sun) in X-ray binary systems, is generally accepted.

From the mathematical point of view, a black hole is a spacetime defined by a four-dimensional metric tensor, that is, a solution of Einstein's equations, with characteristic properties. The simplest black hole is spherically symmetric and non-rotating. It is known as the Schwarzschild black hole, and is described by the metric tensor g_{ab} which is given by

$$\begin{aligned} ds^2 &= \sum_{a=1}^{4}\sum_{b=1}^{4} g_{ab}dx^a\,dx^b \equiv g_{ab}dx^a\,dx^b = \\ &= -\frac{\Delta}{r^2}dt^2 + \frac{r^2}{\Delta}dr^2 + r^2 d\theta^2 + r^2\sin^2\theta\, d\varphi^2 \quad (1.1) \end{aligned}$$

Here ds is the infinitesimal element of proper time, the coordinates are $\{x^a\} = (t, r, \theta, \varphi)$, and we have defined $\Delta = r^2 - 2Mr$ where M is a constant given by $M = GM_{BH}/c^2$ where M_{BH} is the black hole mass and G is Newton's constant. In the following we will always choose so-called geometrised units in which both the speed of light c and G are equal to unity. We will also assume that repated indices indicate summation, as in (1.1).

We are interested in scattering problems involving black holes. In such problems the curvature of spacetime enters not only at the level of the boundary conditions, but also in the equations describing the propagation of the various wave-fields (scalar, electromagnetic or gravitational) that we may be interested in. Therefore the problem of scattering by black holes has more in common with scattering in media with a non-constant index of refraction than scattering by a physical object. In the case of a black hole, it is the curvature of space-time itself which is doing the scattering.

In this article we aim to summarise work in this research area, and relate them to results in familiar contexts such as quantum scattering. We will discuss possible diffraction effects, resonances, and digress on some of the peculiarities of the black-hole problem. It is useful to begin our discussion with the simplest of scattering problems involving black holes; namely, the bending of light rays propagating in a black hole spacetime.

II. CLASSICAL TRAJECTORIES

A. Photon trajectories outside Schwarzschild black holes

Let us consider an astronaut who, while piloting his spaceship towards a Schwarzschild black hole (Figure 1), shines a laser directly out his window, in the positive φ direction. The trajectory of the laser beam can be found by solving the equation for a null geodesic (a line that is "as straight as possible" in the curved spacetime). Hence we are looking for a solution to the geodesic equation

$$\frac{d}{d\lambda}\left(\frac{dx^\alpha}{d\lambda}\right) + \Gamma^\alpha_{\mu\nu}\frac{dx^\mu}{d\lambda}\frac{dx^\nu}{d\lambda} = 0 \quad (2.1)$$

where the Christoffel symbols $\Gamma^\alpha_{\mu\nu}$ are functions of the coordinates $\{x^\alpha\}$. In order to be null, our geodesic must satisfy $x^\mu x_\mu = 0$. Now, if we use the Schwarzschild coordinates introduced in (1.1) we can cast the equation for a null geodesic into the following form:

$$\frac{d\varphi}{dr} = \pm\frac{1}{r^2}\left[\frac{1}{b^2} - \frac{1}{r^2}\left(1 - \frac{2M}{r}\right)\right]^{-1/2} . \quad (2.2)$$

where b is the impact parameter defined by $b = L/E$ where L and E are the angular momentum and the en-

ergy associated with the photon. From equation (2.2) we can deduce the properties of various light trajectories.

FIG. 1: An astronaut maneuvers his rocket ship near a non-rotating black hole.

As the astronaut nears the black hole, the laser beam is deflected more and more by the spacetime curvature — see Figure 2. The curves in Figure 2 are the solutions of equation (2.2) with $\varphi'(b) = 0$ and b ranging from $2.5M$ to $5M$. It should be noted that $r = 3M$ corresponds to a circle. This is known as the unstable photon orbit, and its existence means that our astronauts laser beam will circle the black hole and illuminate his neck! After passing $r = 3M$ the astronaut finds that the laser beam is always deflected into the black hole.

FIG. 2: Light trajectories in the Schwarzschild geometry for various values of the impact parameter b. This shows what happens to a laser beam which shines out the window of a spaceship as it plunges into a (Schwarzschild) black hole. Note the circular 'photon orbit' at $r = 3M$. The (grey) circle at $r = 2M$ represents the event horizon of the black hole.

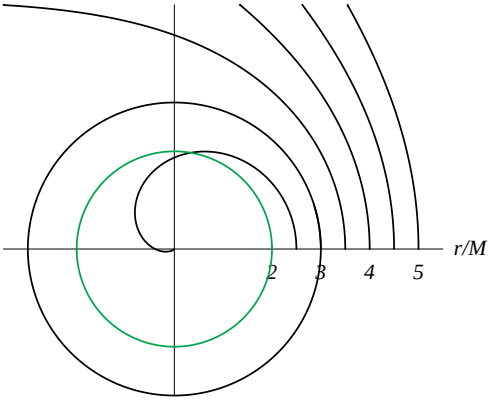

When he reaches $r = 2.1M$, the astronaut applies his rockets in such a way that the spaceship hovers at a constant distance from the black hole, and tries to shine his light at various angles. He then finds that there is still a (small) range of angles at which the light beam can escape the black hole (see Figure 3).

FIG. 3: More light trajectories in the Schwarzschild spacetime. At $r = 2.1M$, the astronaut finds that a light beam from his spaceship can escape the black hole for only a small range of angles. As $r \to 2M$, this becomes a single point.

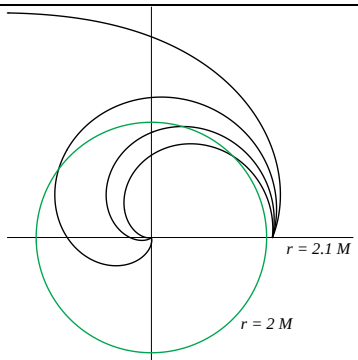

Once the astronaut has resumed his fall towards the black hole, and reached $r \to 2M$, the solid angle into which he must shine his laser in order for the light to escape the black hole has shrunk to a single point. He must aim it in the positive r direction. However, even if he hovers at constant $r = 2M$, the ratio of the light frequency received (ν') by his home planet at (say) $r' = \infty$ to the frequency emitted (ν) is the ratio of the proper times at the two points. This follows from the formula for the *gravitational redshift*:

$$\nu' = \nu(1 - 2M/r). \tag{2.3}$$

From this we see that when $r \to 2M$ the light is completely redshifted away. Therefore any light emitted after the astronaut reaches this limit, whatever the direction, remains inside the black hole. Our space traveller has reached the so-called event horizon, and he can neither escape the black hole nor alert a rescue team of his fate.

B. Bending of Starlight

The above discussion illustrates some of the extreme effects that the curvature of a black-hole spacetime might have on light trajectories. Still, the ideas are relevant also in a more familiar setting. In fact, the first experimental verification of Einstein's theory of general relativity was the measurement of the bending of starlight by the gravitational field of the sun during a solar eclipse of 1919. While the sun is certainly not a black hole, the metric tensor exterior to the surface of the sun is accurately described by (1.1). Thus, in a sense, the first test of general relativity was also the first 'black-hole scattering' experiment.

FIG. 4: The earliest 'black-hole scattering' experiment: deflection of starlight by the sun.

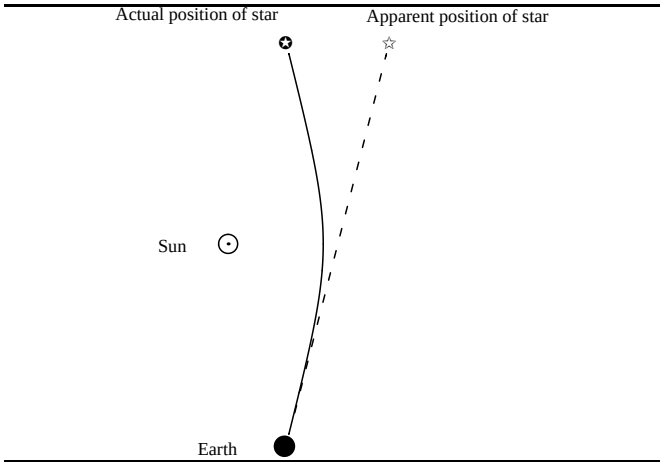

Let us assume that M/r is small ($<< 1$) but not negligible. If we introduce a new variable

$$y = \frac{1}{r}\left(1 - \frac{M}{r}\right) \ , \tag{2.4}$$

we can approximate our equation (2.2) as

$$\frac{d\varphi}{dy} = \frac{1 + 2My}{\left(\frac{1}{b^2} - y^2\right)^{1/2}} + O(M^2/r^2) \ . \tag{2.5}$$

Integration of this leads to

$$\varphi - \varphi_0 = \frac{2M}{b} + \sin^{-1}(by) - 2M\left(\frac{1}{b^2} - y^2\right)^{1/2} \ . \tag{2.6}$$

The initial trajectory was such that $y \to 0$, which means that $\varphi \to \varphi_0$, defining the incoming direction. The smallest value of y that the light ray will ever reach corresponds to $y = 1/b$ when $\varphi - \varphi_0 = 2M/b + \pi/2$. By symmetry the ray will be deflected by an equal amount as it recedes to infinity. Hence, the final result will be $\varphi - \varphi_0 = 4M/b + \pi$, and since the result would have been $\varphi - \varphi_0 = \pi$ if the light ray had followed a straight path, we have a total deflection of

$$\Delta\varphi = \frac{4M}{b} \ . \tag{2.7}$$

This result was first calculated by Einstein, and as noted above, this deflection was measured by Eddington and collaborators in 1919.

C. Gravitational lensing

With enhanced observational capabilities, ranging from large radio telescopes to the repaired Hubble space telescope, astronomers have found plenty of evidence that light often bends as it travels through space. This is known as gravitational lensing. Before discussing some of these observations it is instructive to describe the simplest lensing situation; the case when light from a distant quasar is lensed by a localised mass distribution (treated as a point source with mass M) on its way to the observatory. The relevant geometry is shown in Figure 5. We denote the true angular separation from the lens to be β, consider a light ray that passes the lens at a minimum distance ξ (essentially the impact parameter from the previous section) and is deflected an angle $\alpha = 4M/\xi$ by the spacetime geometry. Assuming that $\xi >> 2M$ we do not need to worry about diffraction effects, and can analyse the problem using simple geometry. Disregarding complicating factors one can show that the condition that the light ray reaches the observer leads to

$$\beta = \theta - \alpha\frac{D_{\rm ds}}{D_{\rm s}} = \theta - \frac{\alpha_0^2}{\theta} \tag{2.8}$$

where we have defined

$$\theta = \frac{\xi}{D_{\rm d}} \ , \qquad \alpha_0^2 = 4M\frac{D_{\rm ds}}{D_{\rm d}D_{\rm s}}$$

and the distances $D_{\rm ds}$, $D_{\rm d}$ and $D_{\rm s}$ are as shown in Figure 5.

FIG. 5: A schematic description of the simplest gravitational lensing geometry. Light rays are bent as the pass by a point source located at point M on their way from the distant source at S to the observer O.

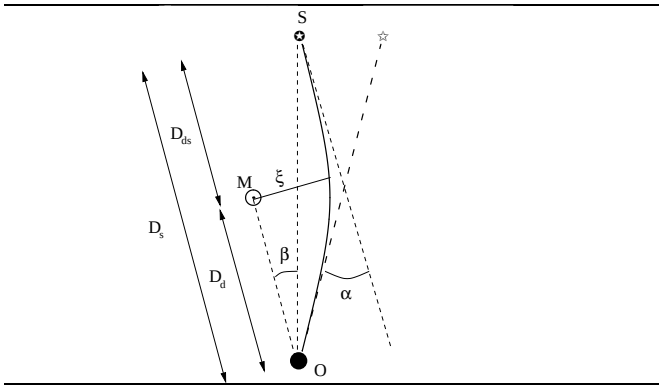

In other words, we solve

$$\theta^2 - \beta\theta - \alpha_0^2 = 0 \tag{2.9}$$

and get

$$\theta_{1,2} = \frac{1}{2}\left(\beta \pm \sqrt{4\alpha_0^2 + \beta^2}\right) \tag{2.10}$$

That is, we always get two solutions of opposite sign. This means that there will typically be one image on each side of the lens. A special case worthy of notice arises when the source, lens and observer are all aligned. Then we have $\beta = 0$ and it is easy to realise that there is then

no preferred plane for the light rays to travel in. Thus the whole ring of angular radius $|\theta| = \alpha_0$ is a solution to the simple lensing equation. This is commonly known as an 'Einstein ring' and, as is easy to see, such images can only occur in lensing by axially symmetric mass distributions.

The above description is obviously idealised in many ways, and in analysing observed gravitational lenses one must consider much more complicated mass distributions, as well as use detailed cosmological models. Still, the above example illustrates the basic principles, and we now turn to some actual observations of gravitational lensing.

The first lensing candidate was observed using a radio telescope at Jodrell Bank in 1979 and is catalogued as 0957+561. It is a typical example of a double image of a distant quasar. When the spectra of the two images were studied it was found that they were remarkably similar, but redshifted to slightly different extent. It was concluded that the two images were extremely unlikely to correspond to separate individual quasars.

Since this first discovery, many other double image systems have been observed. More complicated systems, comprising of further images, have also been found. Among them are the triple image lenses 2016+112 and 0023+171. Perhaps the most unique multiple image case found so far is 2237+0305, more commonly known as the "Einstein cross". In this beautiful system, shown in figure 6, one can see four distinct images.

FIG. 6: The famous "Einstein Cross" is a case where a gravitational lensing by a massive galaxy (central image) leads to four distinct images of a distant quasar. This picture was taken by the William Hershel Telescope in August 1994.

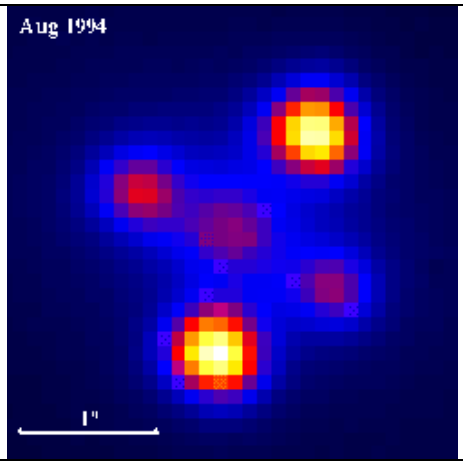

The above examples are all likely examples of lensing by 'point sources'. For extended mass distributions, like galaxies, one would expect to see also arcs and in some unique cases almost complete Einstein rings. The first arcs (Abell 370 and Cl224-02) were actually found when gravitational lenses were still considered a mere theoretical possibility. Since then many further examples of lensed arcs have been discovered, as well as nearly complete rings. One interesting example of the latter is MG1131+0456.

As our observational capabilities continue to improve the list of lensed systems is rapidly growing. New observations provide challenges for the theorists that want to deduce the geometry of the lensing mass distribution as well as understand the nature of the original light source. Ideally, one would also like to be able to use lensing observations of distant quasars to also deduce information about cosmology. Considerable progress in these directions have been made in recent years, and our understanding should continue to improve with the observational data. For further details, we refer the reader to the monograph by Schneider, Ehlers and Falco [1].

III. WAVE SCATTERING

Having discussed some classic examples and exciting observations of the scattering of light by massive bodies we now turn to the issue of possible diffraction effects. Essentially, most models of the gravitational lensing phenomenon are based on "geometrical optics". Therefore one would not expect these calculations to yield any insight into possible wave phenomena. However, as we will see, the extreme nature of black holes lead to the existence of many complicated diffraction effects. To understand these it is essential that we develop a framework for studying the scattering of waves by black holes. From an observational point of view, our main interest will be focussed on electromagnetic and gravitational waves. The latter are particularly interesting since a new generation of gravitational-wave detectors is due to come online in the next few years. It is generally believed that these will make the long-heralded field of gravitational-wave astronomy a reality, and that they will allow us ot make detailed observations of the physics in the immediate vicinity of a black hole [2].

In order to introduce the various concepts involved in studies of the scattering of waves by black holes we will consider the relatively simple case of scalar waves. This may seem like a peculiar choice given that no massless scalar fields have yet been observed in nature. However, it turns out that the main equations governing a weak electromagnetic field, or gravitational waves, in a curved spacetime are essentially the same as the scalar field wave equation (see for example equation (8.18)). Hence, the scalar field serves as a useful model. See Chandrasekhar [3] for an exhaustive study.

A. Scalar Fields in the Schwarzschild geometry

Let us consider a scalar field Φ propagating in the Schwarzschild spacetime, as described by (1.1). The equation governing the evolution of the scalar field is

$$\Box\Phi = \frac{1}{\sqrt{g}}\frac{\partial}{\partial x^\mu}\sqrt{g}g^{\mu\nu}\frac{\partial}{\partial x^\nu}\Phi = 0 \qquad (3.1)$$

where g is the determinant of $g_{\mu\nu}$. Since the Schwarzschild spacetime is spherically symmetric, we may assume a Fourier decomposition

$$\Phi(x^\mu) = \frac{1}{4\pi r}\sum_{l=0}^{\infty}\sum_{m=-l}^{l} e^{-i\omega t}Y_l^m(\theta,\varphi)\hat{\phi}_{lm}(\omega,r) \qquad (3.2)$$

where Y_l^m are the spherical harmonics. If the boundary conditions are cylindrically symmetric, as they would be in the plane-wave scattering problem, the $\varphi = 0$ axis (z-axis) can always be chosen to be the axis of symmetry. We can therefore assume that $\hat{\phi}_{lm}$ to be independent of φ and perform the sum over m, writing

$$\Phi(x^\mu) = \sum_{l=0}^{\infty}(2l+1)e^{-i\omega t}P_l(\cos\theta)\frac{\hat{\phi}_l(\omega,r)}{r} \qquad (3.3)$$

where P_l is a Legendre function.

In the Schwarzschild spacetime the wave equation for the scalar field reduces to the following Schrödinger-type equation for $\hat{\phi}_l$:

$$\frac{d^2\hat{\phi}_l}{dr_*^2} + \left[\omega^2 - V(r)\right]\hat{\phi}_l = 0, \qquad (3.4)$$

where the so-called tortoise coordinate is defined by

$$\frac{d}{dr_*} = \frac{r-2M}{r}\frac{d}{dr} \qquad (3.5)$$

This integrates to

$$r_* = r + 2M\log\left(\frac{r}{2M} - 1\right) \qquad (3.6)$$

and we see that introducing the tortoise coordinate corresponds to "pushing the event horizon of the black hole away to $-\infty$". The effective potential is explicitly given by

$$V(r) = \frac{r-2M}{r}\left[\frac{l(l+1)}{r^2} + \frac{2M}{r^3}\right]. \qquad (3.7)$$

It is positive definite and has a single peak in the range $r_* \in [-\infty,\infty]$, see Figure 7.

A black hole is distinguished by the fact that no information can escape from within the event horizon. Hence, any physical solution to (3.4) must be purely ingoing at the event horizon, that is, at $r = 2M$ ($r_* \to -\infty$). Therefore we seek solutions to (3.4) of form (for a given frequency ω)

$$\hat{\phi}_l \sim \begin{cases} e^{-i\omega r_* + il\pi/2} - S_l(\omega)e^{+i\omega r_* - il\pi/2} & r_* \to \infty \\ T_l(\omega)e^{-i\omega r_*} & r_* \to -\infty \end{cases} \qquad (3.8)$$

where the amplitudes of the scattered and the transmitted waves, S_l and T_l, remain to be determined. Clearly, problems involving waves scattered from a Schwarzschild black hole share many features with scattering problems

FIG. 7: A schematic description of the scattering of waves in the Schwarzschild background. The effective potential of equation (3.4) is shown as a function of r_*. The event horizon of the black hole is located at $r_* = -\infty$. An incident wave I is decomposed into a transmitted component T and a scattered component S.

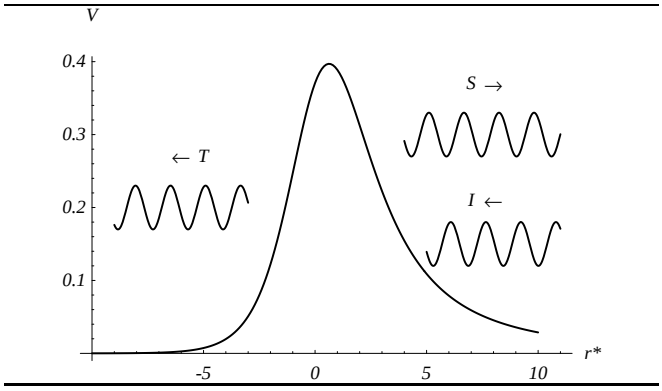

in quantum theory. Hence, we can adopt standard techniques to evaluate S_l and T_l. By conservation of flux it follows that

$$|T_l|^2 = 1 - |S_l|^2 \qquad (3.9)$$

Hence, we need only determine either S_l or T_l. Typical results for S_l are shown in Figure 8.

The nature of S_l can be understood from the following observations. For $\omega << 2M$ the wavelength of the infalling wave is so large that the wave is essentially unaffected by the presence of the black hole. It is only if we "aim" the wave straight at the black hole (recall that the impact parameter follows from $b = L/E \sim l/\omega$) that we can get an appreciable effect. Hence, we expect to have $S_l \to 1$ as $\omega \to 0$. For large frequencies $\omega >> 2M$, the situation is the opposite and we expect to find that $S_l \to 0$ as $\omega \to \infty$. Thus, high frequency waves will be absorbed unless they are aimed away from the black hole.

FIG. 8: Scalar wave scattering coefficient S_l for $l = 0, 1, 2, 3$ as a function of $2M\omega$.

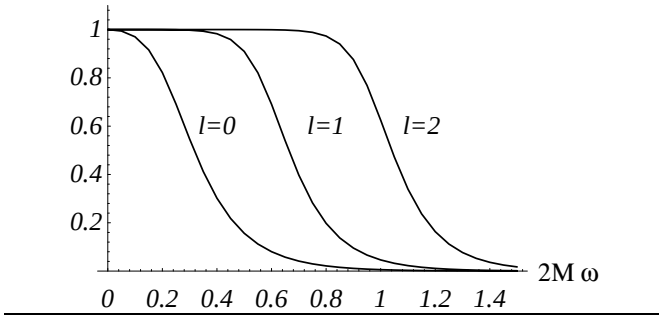

In studies of dynamical black holes one often needs to construct the general solution to (3.4). One can do

this using two linearly independent solutions. These are customarily normalised in a way that differs slightly from (3.8). A first solution (essentially (3.8)) is such that the amplitude of the waves falling across the event horizon are normalised to unity, and one requires the amplitudes of out- and ingoing waves at infinity. This solution is sometimes called the "in"-mode and it can be written

$$\hat{\phi}_l^{\rm in} \sim \begin{cases} e^{-i\omega r_*} \ , & r_* \to -\infty \ , \\ A_{\rm out}(\omega) e^{i\omega r_*} + A_{\rm in}(\omega) e^{-i\omega r_*} \ , & r_* \to +\infty \ , \end{cases} \tag{3.10}$$

Given this solution, a second linearly independent one corresponds to waves of unit amplitude reaching spatial infinity. This is the "up" mode, and it follows from

$$\hat{\phi}_l^{\rm up} \sim \begin{cases} B_{\rm out}(\omega) e^{i\omega r_*} + B_{\rm in}(\omega) e^{-i\omega r_*} \ , & r_* \to -\infty \ , \\ e^{+i\omega r_*} \ , & r_* \to +\infty \ , \end{cases} \tag{3.11}$$

The nature of these two solutions is illustrated in Figure 9.

FIG. 9: The nature of two linearly independent solutions to the scalar wave equation outside a black hole. The in-mode corresponds to purely ingoing waves crossing the event horizon (H^+), while the up-mode corresponds to purely outgoing waves at spatial infinity (I^+).

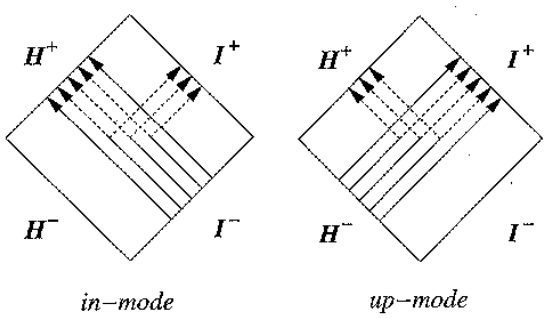

For those unfamiliar with conformal diagrams, a short explanation of Figure 9 is necessary. Suppressing the angular coordinates (θ, ϕ), we make a coordinate transformation in (t, r) such that the half-infinite space exterior to the black hole is mapped onto a finite portion of the plane. The transformation is chosen so that the light cones always intersect at an angle of 45° —much like Mercator's projection of the earth distorts the shape of the continents but preserves the directions North-South and East-West. The four 'points at infinity' are mapped into the diagonal edges as follows: The diamond-shaped

Name	Symbol	Coordinates
Past Horizon	$\mathbf{H}^-$	$r^* = -\infty$, $t = -\infty$
Future Horizon	$\mathbf{H}^+$	$r^* = -\infty$, $t = +\infty$
Past Null Infinity	$\mathbf{I}^-$	$r^* = +\infty$, $t = -\infty$
Future Null Infinity	$\mathbf{I}^+$	$r^* = +\infty$, $t = +\infty$

figures represent the whole of the space-time exterior to the black hole. The various arrows represent the path followed by the incident, transmitted and reflected wave fronts.

B. Plane wave scattering

In order to better understand the physics of black holes we want to formulate a scattering problem analogous to that used to probe the nature of (say) nuclear particles. We want to let a plane wave fall onto the black hole, and investigate how the black hole manifests itself in the scattered wave. This is obviously a model problem, given that we cannot expect to ever be able to compare the calculated scattering cross sections to real observations, but it is still instructive. In particular, it will lead to an unveiling of a deep analogy between black hole physics and well known phenomena such as glory scattering.

However, in formulating this problem we immediately face difficulties. What exactly do we mean by a *plane wave* in a curved spacetime? It turns out that we can answer this question by appealing to the analogous problem of Coulomb scattering. As with the charge in the Coulomb problem, the black hole contributes a long-range potential that falls off as $1/r$ at large distances. The effect of such a long-range potential on the "plane" wave can be accounted for by a simple modification of the standard (flat space) expressions for the scattering amplitude. In the black-hole case we essentially need to introduce r_* in the phase of the plane wave, and we obtain

$$\Phi_{\rm plane} \sim \frac{1}{\omega r} \sum_{l=0}^{\infty} i^l (2l+1) P_l(\cos\theta) \sin\left[\omega r_* - \frac{l\pi}{2}\right] \tag{3.12}$$

as $r_* \to +\infty$ in the case of scalar waves.

C. Phase-shifts and deflection function

Having defined a suitable plane wave, the scattering problem involves finding a solution to (3.4) , *i.e.*, identifying the asymptotic amplitudes $A_{\rm in}$ and $A_{\rm out}$ for a given frequency ω. Then we can extract the scattered wave by discarding the part of the solution that corresponds to the original plane wave. The physical information we are interested in is contained within the scattering amplitude $f(\theta)$, which follows from

$$\Phi \sim \Phi_{\rm plane} + \frac{f(\theta)}{r} e^{i\omega r_*}, \quad \text{as } r_* \to +\infty \ . \tag{3.13}$$

Now letting

$$\Phi - \Phi_{\rm plane} \sim \frac{1}{2i\omega r} e^{i\omega r_*} \sum_{l=0}^{\infty} (2l+1) \left[e^{2i\delta_l} - 1\right] P_l(\cos\theta) \quad \text{as } r_* \to +\infty \ , \tag{3.14}$$

define the (complex-valued) phase-shifts δ_l it is straightforward to show that

$$e^{2i\delta_l} = S_l = (-1)^{l+1}\frac{A_{\rm out}}{A_{\rm in}} \ . \qquad (3.15)$$

From this it follows that the scattering amplitude, that contains all the physical information, is given by

$$f(\theta) = \frac{1}{2i\omega}\sum_{l=0}^{\infty}(2l+1)\left[e^{2i\delta_l}-1\right]P_l(\cos\theta) \ . \qquad (3.16)$$

When discussing the physical quantities that follow from a set of phase-shifts it is natural to use Ford and Wheeler's excellent description of semiclassical scattering from 1959 [4]. In the semiclassical picture the impact parameter b is given by

$$b = \left(l+\frac{1}{2}\right)\frac{1}{\omega} \ . \qquad (3.17)$$

Then each partial wave is considered as impinging on the black hole from an initial distance b away from the axis.

In this description much physical information can be extracted from the so-called deflection function $\Theta(l)$. It corresponds to the angle by which a certain partial wave is scattered by the black hole, and is related to the real part of the phase-shifts;

$$\Theta(l) = 2\frac{d}{dl}{\rm Re}\ \delta_l \ . \qquad (3.18)$$

Here l is allowed to assume continuous real values. We can obtain approximations for $\Theta(l)$ in some limiting cases. For large values of the impact parameter, b, one would expect the value of the deflection function to agree with Einstein's classic result $\Theta \approx -4M/b$, that we derived earlier. As can be seen in Figure 10 this is certainly the case. A numerically determined $\Theta(l)$ rapidly approaches the approximate result as l increases.

A second approximation is intimately related to the existence of a glory in black-hole scattering. Whenever the classical cross section diverges in either the forward or the backward direction a diffraction phenomenon called a glory arises. This phenomenon is well-known in both optics and quantum scattering. In general, backward glories can occur if $\Theta < -\pi$ for some values of b. Whenever the deflection function passes through zero or a multiple of π we have a glory. In the black-hole case one would expect glory scattering to be associated with the unstable photon orbit at $r = 3M$. This essentially means that we would expect a logarithmic singularity in the deflection function to be associated with the critical impact parameter $b_c = 3\sqrt{3}M$. This feature is obvious in Figure 10. Many years ago Darwin [6] deduced an approximate relation between the impact parameter and the deflection function close to this singularity;

$$b(\Theta) \approx 3\sqrt{3}M + 3.48Me^{-\Theta} \ . \qquad (3.19)$$

If we invert this formula and use (3.17) we get Θ as a function of l. As can be seen in Figure 10 this approximation is in excellent agreement with the deflection function obtained from the approximate phase-shifts.

FIG. 10: The deflection function Θ (solid) is shown as a function of l for $\omega M = 10$. For large impact parameters (large l) the approximate results approach the Einstein deflection angle $-4M/b$ (dashed). A logarithmic singularity in Θ is apparent at the critical impact parameter ($l_c \approx 51.5$ here). This feature is associated with the unstable photon orbit at $r = 3M$. Also shown (as a dashed curve) is an approximation obtained by inverting Darwin's formula.

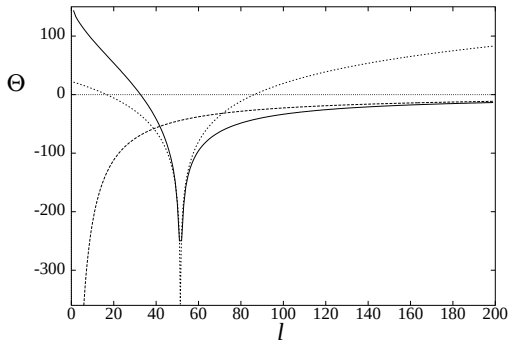

D. The black-hole glory

We now want to proceed to calculate the scattering amplitude through the partial-wave sum (3.16). In doing this, we must proceed with caution since, as in the Coulomb problem, the sum is divergent. This problem is normally avoided by introducing a cutoff where the remainder of the true partial-wave sum is replaced by analytic results for a limiting case. In essence, we extract the contribution from large impact parameters from (3.16) , *i.e.*, replace it by

$$f(\theta) = f_N(\theta) + f_D(\theta) \ , \qquad (3.20)$$

where the long-range (Newtonian) contribution is given by

$$f_N(\theta) = M\frac{\Gamma(1-2iM\omega)}{\Gamma(1+2iM\omega)}\left[\sin\frac{\theta}{2}\right]^{-2+4iM\omega} \ , \qquad (3.21)$$

and

$$f_D(\theta) = \frac{1}{2i\omega}\sum_{l=0}^{\infty}(2l+1)\left[e^{2i\delta_l}-e^{2i\delta_l^N}\right]P_l(\cos\theta) \ , \qquad (3.22)$$

is the part of the scattering amplitude that gives rise to diffraction effects. The Newtonian phase-shifts δ_l^N follow from (cf. the standard Coulomb expression)

$$e^{2i\delta_l^N} = \frac{\Gamma(l+1-2iM\omega)}{\Gamma(l+1+2iM\omega)} \ . \qquad (3.23)$$

The sum in (3.22) is convergent, and we can readily determine the desired physical quantities. The quantity of main physical interest is the differential cross section – the "intensity" of waves scattered into a certain solid angle. It follows from the well-known relation

$$\frac{d\sigma}{d\Omega} = |f(\theta)|^2 \ . \qquad (3.24)$$

A typical example of a scalar wave cross section is shown in Figure 11. This provides a beautiful example of the black-hole glory (the regular oscillations at large angles).

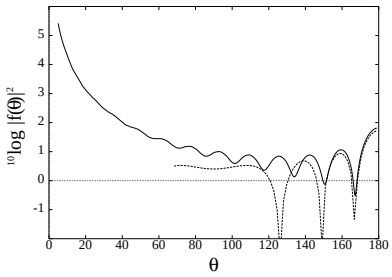

FIG. 11: The scalar wave differential cross section for $\omega M = 2.0$. The oscillations on the backward direction corresponds to the black-hole glory. Also shown is an approximation to the glory oscillations following from equation (3.25).

It is appropriate to discuss the details of the cross section shown in Figure 11 in somewhat more detail. First of all, one would expect the long-range attraction of the gravitational interaction to give rise to a divergent focusing ($\sim \theta^{-4}$) in the forward direction. Secondly, we expect to find that interference between partial waves associated with the unstable photon orbit, *i.e.*, with impact parameters $b \approx b_c = 3\sqrt{3}M$, gives rise to a glory effect in the backward direction (cf. Figure 10). This effect is, of course, prominent in Figure 11. The glory oscillations in the cross section can be approximated by[7]

$$\left.\frac{d\sigma}{d\Omega}\right|_{glory} = 2\pi\omega b^2 \left|\frac{db}{d\theta}\right| J_0^2(\omega b \sin\theta) \ . \qquad (3.25)$$

When combined with the Darwin formula (3.19) this provides a good approximation whenever $\omega M >> 1$ and $|\theta - \pi| << 1$, see Figure 11.

According to the predictions of geometrical optics one might expect to find glory oscillations not only in the backward direction, but also in the forward direction. Partial waves associated with the critical impact parameter may be deflected any multiple of π and so give rise to diffraction close to both $\theta = 0$ and π. Moreover, in Figure 10 we see that the deflection function passes through $\Theta = 0$ for a value of l lower than that associated with the unstable photon orbit (l_c). This means that there should be also a forward glory. However, this feature drowns in the divergence of the cross section that is due to the large l partial waves. Moreover, partial waves corresponding to $l < l_c$ are to a large extent absorbed by the black hole. Hence, the forward glory is exceptionally faint.

IV. TIME-DEPENDENT SCATTERING — RESONANCES

As we have already pointed out, the scattering theory of monochromatic plane waves by a black hole, though interesting, is not likely to have any experimental confirmation soon. The only possibility (as we can see it) would be via diffraction effects observed in gravitational lenses. In order to discuss potentially observable scattering effects we must turn to the closely related problem of the response of the black hole to an initial perturbation. The perturbation response, the black hole's "fingerprints", will only be observable via gravitational waves. Such observations are still outstanding, but the should become reality in the next few years when large scale interferometric gravitational wave detectors (LIGO, VIRGO, GEO600, TAMA300) come online. A typical astrophysical scenario that would produce copious amounts of gravitational waves is a black hole in the act of swallowing a neutron star at the endpoint of binary evolution [2]. The perturbation of the black-hole gravitational field would produce outgoing gravitational radiation which can be detected far from the black hole. We shall see below that this radiation has a characteristic spectrum which indicates the presence of the hole and can be used to deduce its mass and angular momentum. In other words, gravitational-wave observations will bring direct observations of the most elusive of our universe's inhabitants, the black holes.

A. A Green's function approach

We are interested in modelling the response of a black hole to a prescribed initial perturbation. As a model problem we continue with the scalar field, and consider the evolution of the field as an initial-value problem. That is, instead of prescribing the asymptotic character of the field (as in the plane-wave case) we suppose that we are given a specified scalar field at time $t = 0$ and that we want to calculate the future evolution of the field. The time-evolution of a wave-field $\Phi_l(r_*, t)$ follows from

$$\begin{aligned}\Phi_l(r_*, t) &= \int G(r_*, y, t)\partial_t\Phi_l(y, 0)dy \\ &+ \int \partial_t G(r_*, y, t)\Phi_l(y, 0)dy \ , \qquad (4.1)\end{aligned}$$

for $t > 0$. The (retarded) Green's function is defined by

$$\left[\frac{\partial^2}{\partial r_*^2} - \frac{\partial^2}{\partial t^2} - V(r)\right] G(r_*, y, t) = \delta(t)\delta(r_* - y) \ , \quad (4.2)$$

together with the condition $G(r_*, y, t) = 0$ for $t \leq 0$ and the appropriate space boundary conditions. These conditions follow from

$$\frac{\partial G}{\partial r_*} + i\omega G = 0 \ , \quad r \to 2M \qquad (4.3)$$

$$\frac{\partial G}{\partial r_*} - i\omega G = 0 \ , \quad r \to \infty \ . \tag{4.4}$$

Let us take $\hat{G}$ to be the one-sided Fourier transform of G:

$$\hat{G}(r_*, y, \omega) = \int_{0-}^{+\infty} G(r_*, y, t) e^{i\omega t} dt \ . \tag{4.5}$$

This transform is well defined as long as $\mathrm{Im}\,\omega \geq 0$, and the corresponding inversion formula is

$$G(r_*, y, t) = \frac{1}{2\pi} \int_{-\infty+ic}^{+\infty+ic} \hat{G}(r_*, y, \omega) e^{-i\omega t} d\omega \ , \tag{4.6}$$

where c is some positive number (see Figure 12). The Green's function $\hat{G}(r_*, y, \omega)$ can now be expressed in terms of two linearly independent solutions to the homogeneous equation (3.4). The two required solutions are (3.10) and (3.11) as defined earlier, giving the Green's function:

$$\hat{G}(r_*, y, \omega) = -\frac{1}{2i\omega A_{\rm in}(\omega)} \begin{cases} \hat{\phi}_l^{\rm in}(r_*, \omega) \hat{\phi}_l^{\rm up}(y, \omega) \ , & r_* < y \ , \\ \hat{\phi}_l^{\rm in}(y, \omega) \hat{\phi}_l^{\rm up}(r_*, \omega) \ , & r_* > y \ . \end{cases} \tag{4.7}$$

Here we have used the Wronskian relation

$$W(\omega) \equiv \hat{\phi}_l^{\rm in} \frac{d\hat{\phi}_l^{\rm up}}{dr_*} - \hat{\phi}_l^{\rm up} \frac{d\hat{\phi}_l^{\rm in}}{dr_*} = 2i\omega A_{\rm in}(\omega) \ . \tag{4.8}$$

B. Quasinormal modes

The initial-value problem can now, in principle, be approached by direct numerical integration of (3.4) for (almost) real values of ω and subsequent inversion of (4.6). It has proved useful, however, to deform the contour of integration in the complex ω plane using Cauchy's theorem and rewrite the integral as a sum over residues plus a remainder integral. Our first task in this process is to find the position of the poles of the Green's function.

The poles in the radial Green's function (4.7) are located at the simple zeros of $A_{\rm in}$, which we will denote $\{\omega_q\}$. When $\omega = \omega_q$, the distinction between $\hat{\phi}_l^{\rm in}$ and $\hat{\phi}_l^{\rm up}$ disappears, so that, if we demand that our solution to (3.4) be both ingoing at the horizon and outgoing at infinity, and then solve the resulting relation for ω, we know that we have found a pole.

It turns out that the corresponding frequencies, known as the quasinormal modes of the black hole (quasinormal because they are damped as radiation dissipates to infinity and across the event horizon), play a dominant role in the evolution of black hole perturbations. The first indication of this was found by Vishveshwara [8]. He realized that one might be able to observe a solitary black hole by scattering of radiation, provided the black hole left its fingerprint on the scattered wave. So he started "pelting" the black hole with Gaussian wave packets. By tuning the width of the impinging Gaussian Vishveshwara found that the black hole responded by ringing in a very characteristic decaying mode; the slowest damped of the black holes quasinormal modes. Subsequent work (in particular in numerical relativity) has shown that the quasinormal modes always play a prominent role in the dynamical response of a black hole to external perturbations (see Figure 13). Impressive results for head-on collisions of two black holes lead to signals that are almost entirely due to quasinormal mode ringing.

FIG. 12: The integral contour of equation (4.6). If $t > r_*$, the contour can be deformed and the integral can be rewritten as a sum over the poles (crosses) and a remainder integral over the branch cut (zig-zag line).

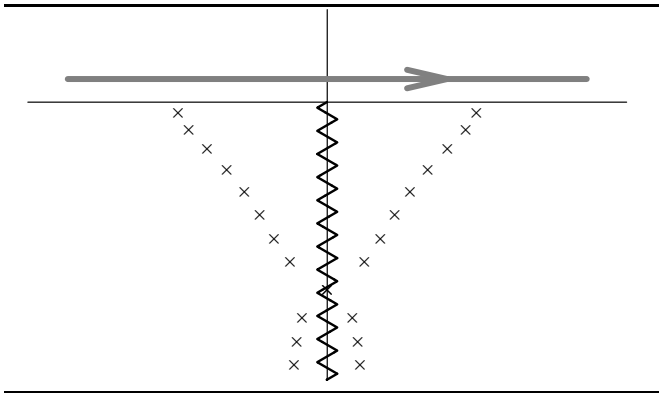

The actual determination of quasinormal mode frequencies is a far from trivial calculation. The quasinormal modes are solutions to (3.4) that satisfy the causal condition of purely ingoing waves crossing the event horizon, while at the same time behaving as purely outgoing waves reaching spatial infinity. Assuming a time-dependence $e^{-i\omega t}$, a general causal solution to (3.4) is given by (3.10) and a quasinormal mode corresponds to $A_{\rm in} = 0$. To identify a mode-solution we must therefore be able to determine a solution that behaves as $e^{i\omega r_*}$ as $r_* \to \infty$, with no admixture of ingoing waves. Assuming that the black hole is stable (we can in fact prove that this must be the case), no unstable mode-solutions should exist so we must require that a mode is damped according to an observer at a fixed location. This means that $\mathrm{Im}\,\omega_q < 0$. The general solution (3.10) is then a mixture of exponentially growing and dying terms. We must, out of all solutions, identify the unique one for which the coefficient of the exponentially dying solution is zero. Several methods have been devised to deal with this difficulty accurately [9]. These methods have been used to investigate the entire spectrum for non-rotating black holes, and also to map out the behaviour of the first ten modes or so as the black hole spins up. The spectrum of gravitational-wave modes of a Schwarzschild black hole is shown in Figure 14.

It is worthwhile to outline one of the most reliable methods (due to Leaver [10]) for calculating black hole quasinormal modes. Write the desired solution to equa-

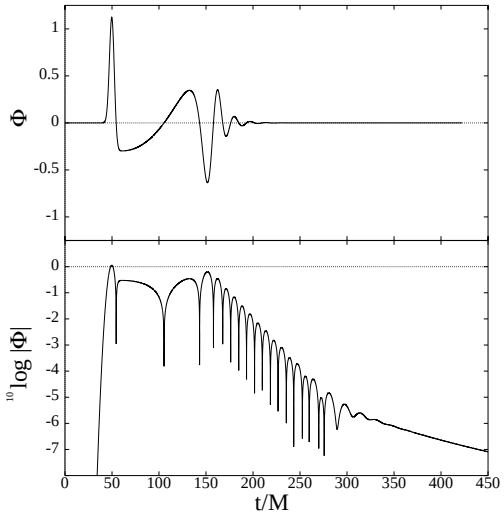

FIG. 13: A recreation of Vishveshwara's classic scattering experiment: The response of a Schwarzschild black hole as a Gaussian wavepacket of scalar waves impinges upon it. The first bump (at $t = 50M$) is the initial Gaussian passing by the observer on its way towards the black hole. Quasinormal-mode ringing clearly dominates the signal after $t \approx 150M$. At very late times (after $t \approx 300M$) the signal is dominated by a power-law fall-off with time. This late time tail arises because of backscattering off of the weak potential in the far zone. As such, it is not an effect exclusive to black holes. A similiar tail will be present also for perturbed stars.

tion (3.4) as an infinite sum

$$\hat{\phi}_l^{\rm in} = (r-2M)^{\rho}(2M/r)^{2\rho}e^{-\rho(r-2M)/2M}\sum_{n=0}^{\infty} a_n \left(\frac{r-2M}{r}\right)^n \tag{4.9}$$

where $\rho = -i2M\omega$. The recurrence relations between the a_n are given by Leaver:

$$\alpha_n a_{n+1} + \beta_n a_n + \gamma_n a_{n-1} = 0, \tag{4.10}$$

where

$$\begin{aligned}\alpha_n &= n^2 + 2n(\rho+1) + 2\rho + 1\\ \beta_n &= -[2n^2 + 2n(4\rho+1) + 8\rho^2 + 4\rho + l(l+1) - s^2 + 1]\\ \gamma_n &= n^2 + 4n\rho + 4\rho^2 - s^2\end{aligned}$$

and s is the spin of the field. Now one can note that the coefficient $A_{\rm in}$ has a zero whenever the sum $\sum a_n$ converges. This requirement translates into an continued-fraction equation involving the coefficients α, β and γ:

$$\left[\beta_q - \frac{\alpha_{q-1}\gamma_q}{\beta_{q-1}-}\frac{\alpha_{q-2}\gamma_{q-1}}{\beta_{q-2}-}\cdots\frac{\alpha_0\gamma_1}{\beta_0}\right] = \left[\frac{\alpha_q\gamma_{q+1}}{\beta_{q+1}-}\frac{\alpha_{q+1}\gamma_{q+2}}{\beta_{q+2}-}\frac{\alpha_{q+2}\gamma_{q+3}}{\beta_{q+3}-}\cdots\right]. \tag{4.11}$$

Here $q = 1, 2, 3, \ldots$ is the mode number. Solving this equation numerically (still a non-trivial task!) for ω_q gives the quasinormal modes (see Figure 14).

FIG. 14: The complex quasinormal mode frequencies corresponding to gravitational perturbations (for $l = 2$ and 3) of a Schwarzschild black hole. These correspond to the positions of the poles of the radial Green's function (equation 4.7) in the complex $2M\omega$ plane.

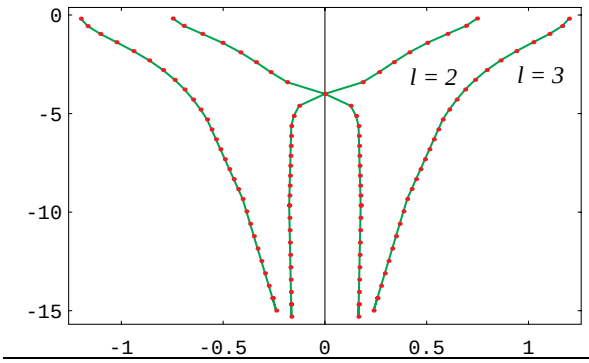

C. Mode excitation

Having located the quasinormal modes we want to evaluate the contribution of each mode to the emerging signal. Ideally one would like to be able to quantitatively account for the contribution to a signal from each individual quasinormal mode. Thus we want to construct the mode-contribution to the Green's function (4.6), combine it with the relevant initial data an extract the corresponding signal using (4.1). To do this is largely a (rather involved) numerical exercise. In the end one finds that the quasinormal modes account for the main part of the signal after a certain time, essentially the time it takes for a part of the initial data to travel from its original position y to the black hole, and then for the scattered wave to reach the observer at r_*. Thus we expect the modes to generally dominate for (roughly) $t - r_* - y > 0$.

It is helpful to introduce a simplifying approximation at this stage. Let us assume that the initial data has support only far away from the black hole, and that the observer is also located in the far zone. Then we can can replace the solutions $\hat{\phi}_l$ in (4.7) by their asymptotic behaviour at large r_* and readily evaluate the mode contribution to the Green's function. Since $A_{\rm in}(\omega)$ has a simple zero at $\omega = \omega_q$, it is useful to define a quantity α_q by

$$A_{\rm in}(\omega) \approx (\omega - \omega_q)\alpha_q\ , \tag{4.12}$$

in the vicinity of the pole. Then it follows from the residue theorem (and the fact that modes in the third and fourth quadrant are in one-to-one correspondence, see Figure 14) that the total contribution from the modes

to the time-domain Green's function can be written

$$G^Q(r_*, y, t) = \mathrm{Re}\left[\sum_{q=0}^{\infty} B_q e^{-i\omega_q(t-r_*-y)}\right] . \qquad (4.13)$$

Here we have defined

$$B_q = \frac{A_{\mathrm{out}}(\omega_q)}{\omega_q \alpha_q} . \qquad (4.14)$$

The sum in (4.13) is over all quasinormal modes in the fourth quadrant of the ω-plane. That this expression provides an accurate representation of the mode-excitation (as long as our assumptions are valid) has been demonstrated.

At this point it is relevant to comment on the fact that the quasinormal modes are, even though there is an infinite set of modes for each l, not complete. That is, a mode sum such as (4.13) should not be expected to represent the entire black-hole signal for given initial data. It will typically not be useful at early times, and it cannot represent the power-law tail that dominates at very late times, see Figure 13. However, the mode-contribution is still highly relevant, and results like (4.13) can help us understand the dynamics of black holes better. Furthermore, expression (4.13) allows us to study the convergence of the mode-sum in a simple way. It has been shown that (again under the assumptions of the "asymptotic approximation") that the mode sum converges for $t - r_* - y > 0$.

D. Useful approximations

The quasinormal modes provide (at least in principle) a unique way of identifying black holes and deducing their mass and rate of rotation. Given this, it instructive to have simple approximations of the most important mode-frequencies. We can readily arrive at such expressions by recalling that the black hole problem is essentially one of scattering off a single potential peak (close to $r = 3M$). It is commonly accepted that scattering resonances (the quantum analogues of quasinormal modes) arise for energies close to the top of a potential barrier. This immediately leads to the approximation

$$\mathrm{Re}\ \omega_0 \approx \frac{1}{3\sqrt{3}M}\left(l + \frac{1}{2}\right) . \qquad (4.15)$$

This is a good approximation of the fundamental Schwarzschild quasinormal (gravitational wave) mode for large l. For the imaginary part of the frequency—in quantum language: the lifetime of the resonance—the curvature of the potential at the peak contains the relevant information. Schutz and Will [11] used the WKB approximation to infer that

$$\mathrm{Im}\ \omega_0 \approx -\frac{\sqrt{3}}{18M} , \qquad (4.16)$$

which is accurate to within 10 percent for the fundamental mode.

Let us translate the results for the fundamental gravitational-wave quasinormal mode of a nonrotating black hole into more familiar units. We then get a frequency

$$f \approx 12\mathrm{kHz}\left(\frac{M_\odot}{M}\right) , \qquad (4.17)$$

where $M_\odot$ represents the mass of the Sun, while the associated e-folding time is

$$\tau \approx 0.05\ \mathrm{ms}\left(\frac{M}{M_\odot}\right) . \qquad (4.18)$$

The quasinormal modes of a black hole are clearly very shortlived. In fact, we can compare a black hole to other resonant systems in nature by considering the quality factor

$$Q \approx \frac{1}{2}\left|\frac{\mathrm{Re}\ \omega_q}{\mathrm{Im}\ \omega_q}\right| . \qquad (4.19)$$

Our quasinormal-mode approximations then lead to $Q \approx l$. This should be compared to the result for the fluid pulsations of a neutron star: $Q \sim 1000$, or the typical value for an atom: $Q \sim 10^6$. A Schwarzschild black hole is clearly a very poor oscillator.

V. COMPLEX ANGULAR MOMENTUM APPROACH

As early as 1972 there was an intriguing suggestion (due to Goebel[12]), that the black-hole resonant modes could have the following physical interpretation: a standing wave could establish itself along the stable photon orbit at or near radius $r = 3M$. Of course this standing wave is not stable but would decay by radiating away energy. Unlike the quasi-normal modes, Goebel's standing waves correspond to poles of the Green function in the complex *angular momentum* plane. Thus we need to extend our previous analysis to allow for complex values of l. That this leads to a powerful description of many scattering problems is well known [13]. The complex angular momentum paradigm has been much investigated in acoustical and electromagnetic scattering, but has received scant attention in the context of black holes.

A. Cross sections

Let us begin by reviewing the theory of complex angular-momentum (CAM) scattering. Let $F(l + 1/2)$ be any function which is analytic in the neighbourhood of the positive real l axis. Then, by Cauchy's theorem, we may write:

$$\sum_{l=0}^{\infty}(-1)^l F(\lambda) = \frac{i}{2}\oint_C \frac{F(\lambda)}{\cos\pi\lambda}\, d\lambda$$

where $\lambda = l + 1/2$. We apply this transformation to equation (3.16), writing

$$f(\theta) = \frac{1}{2\omega} \oint_C \frac{\lambda[S_l - 1]P_l(-\cos\theta)}{\cos \pi\lambda}\, d\lambda.$$

We deform the contour C away from the real l axis, rewriting f as the sum over the poles in S_l and a background integral (see Figure 15).

$$f(\theta) = f_P + f_B = \frac{-i\pi}{\omega} \sum_n \frac{\lambda_n r_n}{\cos \lambda_n} + \frac{1}{2\omega} \int_\Gamma \frac{\lambda[S_l - 1]P_l(-\cos\theta)}{\cos \pi\lambda}\, d\lambda. \quad (5.1)$$

Here r_n is the residue associated with the pole l_n, defined by

$$S_l \approx \frac{r_n}{l - l_n}\ , \quad (5.2)$$

in the vicinity of the nth pole. Even though we will not consider the 'background integral' further in this article, it is worth mentioning that it can be approximated using the saddle point method.

FIG. 15: Integration contours in the complex $\lambda(= l + 1/2)$-plane used in the derivation of the CAM representation for the scattering amplitude, equation (5.1). C is the original contour used in the integral representation for the scattering amplitude. The relevant contour for the background integral in the CAM picture is Γ. The Regge poles λ_n are all situated in the first quadrant. Their contribution is accounted for by the residue-theorem.

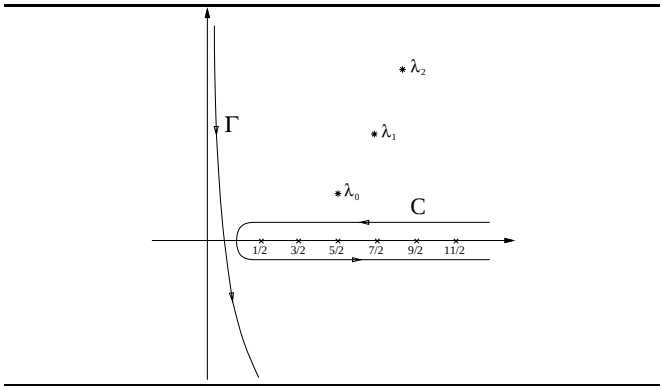

The poles of $S(\lambda)$ are known as Regge poles and for the black hole potential one can show (Andersson and Thylwe, 1994) that they are all located in the first quadrant of the complex λ-plane. If If we compare the solution for one of the Regge poles to that of a quasinormal mode we see that they are rather similar. Both solutions satisfy purely "outgoing" wave boundary conditions. Hence, methods used for finding the quasi-normal mode frequencies can be adapted to find the Regge poles. One can show that these poles are all located in the first quadrant of the complex λ-plane. Typical results for the first few poles are shown in Figure 16.

FIG. 16: The trajectory of the Regge poles $l_n(\omega)$ ($n = 1, 2, 3, 4$) followed in the complex l plane from $\omega M = 0$ (on the line $l = -1/2$) to $\omega M = 5$.

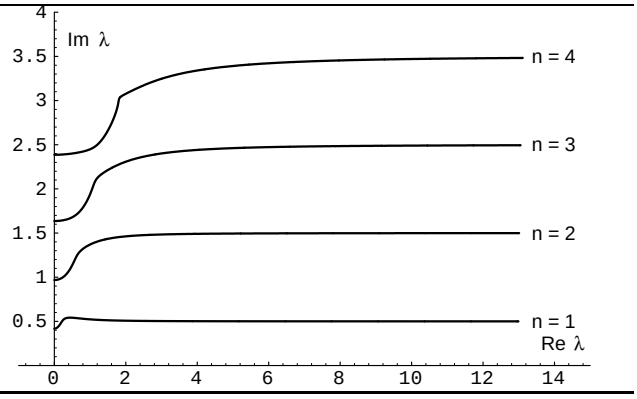

VI. PHYSICAL INTERPRETATIONS

An important aspect of the CAM description of scattering is that each Regge pole has a clear interpretation. To realize this two approximations for the Legendre functions are useful:

For θ not close to 0 and $|\lambda_n| >> 1$ we can use the formula

$$P_{l_n}(-\cos\theta) \approx \left(\frac{\pi - \theta}{\sin\theta}\right)^{1/2} J_0\left(\lambda_n(\pi - \theta)\right)\ , \quad (6.1)$$

when evaluating the Regge-pole sum (5.1). This is especially interesting since we know that black-hole cross sections show a prominent glory in the backward direction, see Figure 11. It is commonly understood that glories are characterized by Bessel-function type oscillations, cf. (3.25). When numerical results for the Regge pole with the smallest imaginary part (for a given ω) is used in (6.1) we get a good approximation to the glory oscillations in the black-hole cross section.

Alternatively, we can use an asymptotic approximation for the Bessel function in (6.1). We then get

$$P_{l_n}(-\cos\theta) \approx \frac{e^{i\lambda_n(\pi-\theta) - i\pi/4} + e^{-i\lambda_n(\pi-\theta) + i\pi/4}}{\sqrt{2\pi\lambda_n \sin\theta}} \quad (6.2)$$

for $|\lambda_n \sin\theta| \to \infty$. From this formula it follows that we may interpret each Regge state as a combination of two surface waves travelling around the scattering centre (the black hole) in opposite directions. The angular velocity of each wave is proportional to $1/\mathrm{Re}\ \lambda_n$, and as they propagate around the black hole the waves decay exponentially. The imaginary part of λ_n is clearly associated with the inverse of the "angular life" of each surface wave. It also follows, since $\mathrm{Im}\ \lambda_n > 0$, that the amplitude of the first term in (6.2) is, in general, smaller that the second term. Only for $\theta \approx \pi$ do the two amplitudes have similar magnitude. Hence, one would expect interference effects to be more pronounced in the backward direction. Moreover, it is easy to show that the anticipated diffraction

oscillations will have a period of $\pi/\mathrm{Re}\ \lambda_n$. Again, this result approximates the features seen in the black-hole cross section rather well.

TABLE I: "Angular life" and impact radius (R_n) for the first few Regge poles for $\omega M = 2$. It should be remembered that the impact parameter associated with the unstable photon orbit at $r = 3M$ is roughly $5.196M$.

n	Impact radius (M)	Angular life (degrees)
0	5.194	114
1	5.207	38
2	5.234	23

We can also use the standard localization principle (cf. the definition of the impact parameter)

$$\mathrm{Re}\ \lambda_n \approx \omega R_n \ , \tag{6.3}$$

to infer that the real part of each pole position is associated with the distance from the black hole at which the angular decay occurs. In the case of a Schwarzschild black hole one would expect such surface waves to be localized close to the unstable photon orbit at $r = 3M$ [or, strictly speaking, the maximum of the effective potential in (3.4)]. This would correspond to $R_n = 3\sqrt{3}M \approx 5.196M$. As can be seen from Table I the first Regge pole for various frequencies leads to a value of R_n that is close to the impact parameter for the photon orbit.

A. Sample results

Although the physical interpretations discussed above are suggestive and agree well with the partial-wave results for the cross section we should also compute the actual cross sections before assessing the usefulness of the CAM approach to black-hole scattering. In Figure 17 we show the contribution to the the pole-sum f_P from the first three Regge poles for $\omega M = 2.0$. The results are compared to the partial-wave cross section as computed from the partial-wave sum (Figure 11). To obtain the Regge-pole contributions we have used the asymptotic formula (6.2) for the Legendre functions.

From the data shown in Figure 17 we make two observations: i) For large scattering angles ($\theta \geq 40°$) the pole sum in (5.1) is dominated by the Regge pole with the smallest imaginary part. Each consecutive pole gives a contribution that is roughly two orders of magnitude smaller than that of the preceding pole. This means that only one Regge pole need be included in a reasonably accurate description of the black-hole glory. ii) For smaller angles ($\theta \leq 40°$) the first three terms in the pole sum are of the same order of magnitude. This is consistent with the interpretation of $1/\mathrm{Im}\ \lambda_n$ as the "angular life", see Table I.

In conclusion, we have shown that the Regge states can be interpreted as surface waves that travel around the black hole. At the same time the waves decay at a rate related to the imaginary part of the Regge pole position. We have also seen that the glory oscillations that arise for large scattering angles in the black-hole case are naturally described in the CAM representation. In the specific example presented (for $\omega M = 2.0$) a single Regge pole accounts for all large-angle structure in the scattering cross section.

FIG. 17: The differential cross section for $\omega M = 2.0$ as obtained from the phase-shifts (solid line) is compared to the contribution from each of the first three Regge poles (dashed lines).

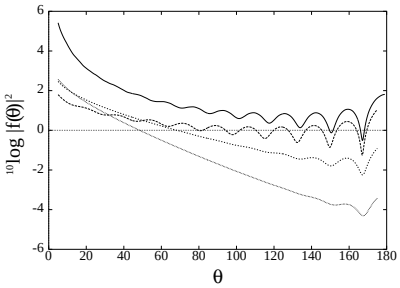

VII. QUANTUM EFFECTS

We will now turn to another extreme scale in physics, the level where the classical theory of general relativity breaks down and it must somehow be married to quantum theory. We will not attempt to describe the ongoing attempts to formulate theory of quantum gravity in detail. Rather, we want to point out that one can gain some insights into quantum gravity (at the semiclassical level) using concepts and techniques very similar to those we have discussed above. In fact, several interesting effects bear a great resemblance to various scattering scenarios. Since we will only skim the surface of a vast area of research, we refer the reader to the monograph by Frolov and Novikov [14] for references and more details.

A. Hawking radiation

Consider Figure 18. A cloud of pressureless dust undergoes collapse to form a black hole. The wiggling lines represent high-frequency waves associated with a massless field (scalar, neutrino, photon, graviton). We suppose that the space is initially indistinguishable from Minkowski space and that the field is in the vacuum state. Now consider the evolution of a high-frequency wave packet that is a part of the spectrum of (Minkowski) vacuum fluctuations. We follow the evolution of the packet which, after the collapse, is localised just outside

FIG. 18: The Hawking effect: when dust collapses to form a black hole, high-frequency vacuum fluctuations near the horizon lead to radiation which can escape to infinity.

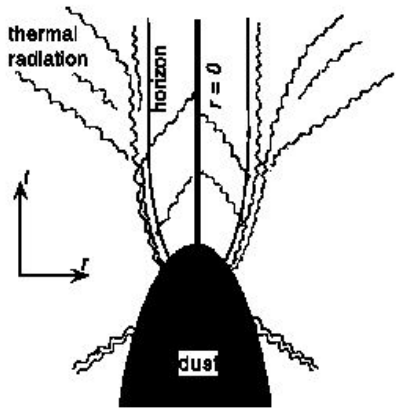

the black hole's horizon at $r = 2M$.

The packet can be spectrally decomposed into a component which is ingoing and another which (eventually) can escape to infinity. Hawking [15] showed that, when viewed from infinity, the spectrum of the escaping radiation is thermal with temperature $T_H = \hbar/(k_B 8\pi M)$. That is, if we Fourier-decompose the radiation escaping to infinity and use the standard definition of the vacuum state, we find that the total number of particles in the mode (n) is

$$N_{(n)} = |T_{(n)}|^2/(e^{\hbar\omega/(k_B T_H)} \mp 1)$$

Here (n) is a general index which represents all quantum numbers and the sign is taken for negative for integer and positive for half-integer spin fields.

We see the connection with scattering theory when we write the expression for the total (scalar) luminosity of the black hole due to Hawking radiation:

$$L = \frac{\hbar}{2\pi}\int_0^\infty \frac{\omega\ d\omega}{e^{\hbar\omega/k_B T_H} - 1}\sum_{l=0}^{\infty}(2l+1)|T_l(\omega)|^2.$$

There are similar formulas for quantum fields of other spins. For a stellar-mass black hole, this is

$$L_{\rm scalar} = 7.44\times 10^{-5}\hbar/M^2$$

Reverting momentarily to cgs units, we can express the luminosity for a field of spin s as

$$L_s = \alpha_s \cdot 4.09\times 10^{-17}\left(\frac{M_\odot}{M_{\rm BH}}\right)^2 {\rm ergs/sec}.$$

where $M_\odot$ is the mass of the sun, and the α_s are given in Table II. Clearly the Hawking effect is too small to ever detect for a black hole of near stellar mass. But the effect may be appreciable for much smaller black holes conceivably created in the early universe. Such primordial black holes would radiate at an appreciable level, and there have been speculations that one might be able to observe bursts of radiation as these black holes evaporate. As yet this effect has, however, not been observed.

field	spin s	$\alpha_s = LM^2/\hbar$
scalar	0	7.44×10^{-5}
neutrino	1/2	8.18×10^{-5}
photon	1	3.37×10^{-5}
graviton	2	0.38×10^{-5}

TABLE II: Black hole luminosity as a function of field spin s

B. Stress-energy tensors

It must be emphasised that the Hawking radiation emitted by the black hole is not produced by the process of collapse but is feature of the field vacuum state in the new spacetime, which now contains a black hole. One of the lessons of quantum field theory in curved spacetime is that we must mistrust the abstract concept of 'particle' and concentrate on physically measurable quantities such as the energy content of the field in a particular state, that is, the stress-energy tensor of the quantum field, written $\langle\hat{T}_\mu{}^\nu\rangle$. It turns out that one can determine the stress-energy tensor via a differential operator acting on the black-hole perturbation Green's function that we have introduced earlier.

It will be useful for what follows to define the *Tolman local temperature*

$$T_{\rm loc} = T_H g_{00}^{-1/2} = T_H/\sqrt{1-2M/r}.$$

A massless scalar field at temperature T has

$$\langle\hat{T}_\mu{}^\nu\rangle_\flat = \frac{\pi^2}{90}T^4{\rm diag}(-3,1,1,1)$$

in flat space. A gas of scalar particles in equilibrium exterior to a spherical body should have

$$\langle\hat{T}_\mu{}^\nu\rangle = \frac{\pi^2}{90}T_{\rm loc}^4{\rm diag}(-3,1,1,1)$$

that is, T is replaced by the local temperature. This expression diverges as $r\to 2M$.

The most obvious choice for the vacuum state exterior to a black hole is the state that, at infinity, resembles as much as possible the Minkowski vacuum state. This state, called the Boulware state, is the vacuum state appropriate for a field outside of a spherical body which is larger than its Schwarzschild radius, such as a neutron star. When $\langle\hat{T}_\mu{}^\nu\rangle$ is calculated in this state it has the asymptotic form

$$\langle\hat{T}_\mu{}^\nu\rangle_B \sim -\frac{\pi^2}{90}T_{\rm loc}^4{\rm diag}(-3,1,1,1) \qquad r\to 2M.$$

In other words, the energy density is negative infinite on $\mathbf{H}^+$ and $\mathbf{H}^-$, cf. Figure 9. Note that this infinity has nothing to do with renormalisation: the divergences in $\langle \hat{T}_\mu{}^\nu \rangle$ have already been removed using covariant, state-independent methods. The presence of a singularity in the stress-energy tensor, even when measured by a freely-falling observer, is unphysical and we conclude that the Boulware state cannot be the ground state of a field exterior to a black hole.

If we are interested in a black hole formed by stellar collapse, we would like the stress-energy tensor to (at least) be regular on $\mathbf{H}^+$ and to tend to the Minkowski vacuum tensor on $\mathbf{I}^-$. The price we pay for this requirement is that the tensor is singular on $\mathbf{H}^-$. (Of course, in the case of stellar collapse, $\mathbf{H}^-$ does not exist.) In addition, at $\mathbf{I}^+$ we have an outflow of thermal radiation as described in the preceding section. This state is called the Unruh state.

If we demand that the stress-energy tensor be regular on both $\mathbf{H}^-$ and $\mathbf{H}^+$ the Hartle-Hawking state, and is appropriate for a spacetime with an eternal black hole in equilibrium with a thermal bath of radiation at the Hawking temperature. The stress tensor has the form:

$$\langle \hat{T}_\mu{}^\nu \rangle_H = \frac{\pi^2}{90} T_{\rm loc}^4 \,{\rm diag}(-3,1,1,1) \left[1 - \left(\frac{2M}{r}\right)^6 \left(4 - \frac{6M}{r}\right) \right] + \text{finite}$$

where 'finite' is a correction everywhere finite and of order r^{-6} for large r. Despite its appearence, $\langle \hat{T}_\mu{}^\nu \rangle_H$ is finite at $r = 2M$.

We see then that the three 'vacuum' states correspond to different physical situations, and that it is not possible to define a state which has the properties which we naturally associate with the vacuum. Although we rejected the Boulware state because of infinite energy on the horizon, the Hartle-Hawking state also has infinite energy, which is contained in the heat bath at infinity. The Unruh state, the most 'realistic' state, is appropriate for an eternally evaporating black hole of constant mass. A real black hole will lose mass by evaporation, evolving to an unknown final state. This unsatisfactory situation will only be resolved by a full quantum theory of gravity.

VIII. THE KERR BLACK HOLE

So far we have only considered the simplest class of black holes, namely those described by the spherically symmetric Schwarzschild solution to Einstein's equations. There are other kinds of black holes as well. In order to generalise our discussion to the case of greatest physical interest we must allow our black hole to rotate. Due to conservation of angular momentum during the gravitational collapse one would expect most newly born black holes to spin very fast. Then the resultant spacetime metric will no longer be spherically symmetric. The corresponding solution to Einstein's equations was discovered by Kerr, and the metric is usually written

$$ds^2 = -\frac{\Delta}{\rho^2}[dt - a\sin^2\theta d\varphi]^2 + \frac{\sin^2\theta}{\rho^2}[(r^2+a^2)d\varphi - a\,dt]^2 + \frac{\rho^2}{\Delta}dr^2 + \rho^2 d\theta^2 \qquad (8.1)$$

where

$$\Delta = r^2 - 2Mr + a^2, \qquad \rho^2 = r^2 + a^2\cos^2\theta$$

Here a is a parameter representing the angular momentum per unit mass. When a equals zero the Kerr metric reduces to the Schwarzschild metric. The event horizon of a rotating black hole corresponds to the outer solution to $\Delta = 0$, and is given by

$$r_+ = M + \sqrt{M^2 - a^2} \leq 2M. \qquad (8.2)$$

In studying scattering from rotating black holes all the concepts we have introduced for non-rotating black holes remain useful. Thus we only need to comment on how these results are affected by the black holes rotation. It is natural to begin by discussing the nature of light trajectories in the Kerr spacetime.

A. Null geodesics in the Kerr geometry

A description of the general trajectories of a particle moving in the Kerr geometry is considerably more complicated than the Schwarzschild case, but because of the axial symmetry one would still expect $p_\theta = 0$ for motion in the equatorial plane (p_μ represents the four-momentum of a photon). If a particle is initially moving in the equatorial plane, it should remain there. In the Schwarzschild case we could always, because of the spherical symmetry, orient our coordinate system in such a way that a study of equatorial trajectories covered all possible cases. For rotating black holes, we no longer do this and an equatorial trajectory is a very special case. Nevertheless, they provide a useful starting point for an exploration of particle motion around a rotating black hole.

Because the Kerr geometry is stationary and axisymmetric, we will still have the two constants of motion $p_t = -E$ and $p_\varphi = L_z$, the "energy measured at infinity" and the component of the angular momentum parallell to the symmetry axis of the spacetime. Given this we can immediately deduce two equations of motion

$$p^t = \frac{dt}{d\lambda} = \frac{(r^2+a^2)^2 - a^2\Delta\sin^2\theta}{\Sigma\Delta}E - \frac{2aMr}{\Sigma\Delta}L_z \qquad (8.3)$$

$$p^\varphi = \frac{d\varphi}{d\lambda} = \frac{2aMr}{\Sigma\Delta}E + \frac{\Delta - a^2\sin^2\theta}{\Sigma\Delta\sin^2\theta}L_z\ , \qquad (8.4)$$

where $\Sigma^2 = (r^2+a^2)^2 - a^2\Delta\sin^2\theta$.

We will restrict our attention to photons moving in the equatorial plane. Then the above formulae together with $p_\mu p^\mu = 0$ and $p_\theta = 0$ lead to an equation for the radial motion that can be factorized as

$$\left(\frac{dr}{d\lambda}\right)^2 = \frac{(r^2+a^2)^2 - a^2\Delta}{r^4}(E-V_+)(E-V_-) \ , \quad (8.5)$$

where we have defined

$$V_\pm(r) = \frac{2aMr \pm r^2\Delta^{1/2}}{(r^2+a^2)^2 - a^2\Delta}L_z \ . \quad (8.6)$$

By expanding these potentials in inverse powers of r we see that they fall off as $1/r$ as $r\to\infty$ (as in the Schwarzschild case), but the effect of rotation enters at order r^{-3}. This means that the rotation of the black hole has little effect on a distant photon. But as the photon approaches the black hole the potentials have a much stronger influence and we can distinguish two different cases. The way that the rotation of the black hole affects an incoming photon depends on direction of L_z relative to the sense of rotation of the black hole.

In the case when $aL_z > 0$, when the photon moves around the black hole in a prograde orbit, we get the situation illustrated in Figure 19. Then we can see from (8.6) that

$$V_- = 0 \text{ at } r = 2M \ , \quad (8.7)$$

$$V_+ = V_- = \frac{aL_z}{2Mr_+} = \omega_+ L_z \text{ at } r = r_+ \ , \quad (8.8)$$

where we have defined the angular velocity of the horizon ω_+.

FIG. 19: The effective potentials for a photon moving in the equatorial plane of a rotating black hole. The figure illustrates the case when the photon has angular momentum directed in the same sense as the rotation of the hole ($a = 0.5M$). The corresponding figure for a retrograde photon (with $aL_z < 0$) is obtained by turning this figure upside-down.

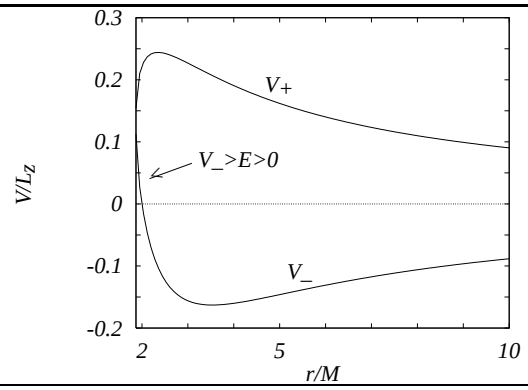

Since the lefthand side of (8.5) must be positive (or zero) we can infer that the photon must either move in the region $E > V_+$ or in $E < V_-$. In the first case the result is familar. An incoming photon from infinity can either be scattered by, or plunge into, the black hole. But what about the region $V_- > E > 0$ that would also seem to be accessible (cf. Figure 19)? An analysis of this possibility requires some care. It turns out that it is not sufficient to require that $E > 0$, as one might intuitively think. The reason for this is quite easy to understand: E is the energy measured at infinity, and as we get closer to the black hole it becomes a less useful measure of what is going on. In order to understand the properties of light trajectories in the vicinity of a spinning black hole, we need an observer located close to the horizon to do our measurements for us.

A convenient choice of local observer is one that has zero-angular momentum and resides at a fixed distance from the black hole (at constant r). Such Zero-Angular Momentum Observers (ZAMOs) were first introduced by Bardeen [16]. (It should be noted that a ZAMO does not follow a geodesic, and consequently must maintain its position, say, by means of a rocket.) The suggested character of a ZAMO means that it must have a four-velocity

$$u^t = A \ , \qquad u^\varphi = \omega A, \qquad u^r = u^\theta = 0 \ . \quad (8.9)$$

The unknown coefficient A is specified by the requirement

$$u_\mu u^\mu = -1 \ , \quad (8.10)$$

and we find that

$$A^2 = \frac{g_{\varphi\varphi}}{(g_{\varphi t})^2 - g_{tt}g_{\varphi\varphi}} \ . \quad (8.11)$$

We are now equipped to address the question of photons in the region $V_- > E > 0$ in Figure 19. A ZAMO will measure the energy of a photon as

$$E_{\rm zamo} = -p_\mu u^\mu = -(p_t u^t + p_\varphi u^\varphi) = A(E - \omega L_z) \ . \quad (8.12)$$

This "locally measured" energy is the one that we must require to be positive definite, which means that we must have $E > V_+$ in Figure 19. In other words, the possibility $V_- > E > 0$ is not physically acceptable and we can conclude that the case $aL_z > 0$ only contains the same types of photon trajectories as we found in the Schwarzschild case.

This is not, however, true for the case when $aL_z < 0$, when the photon is inserted in a retrograde orbit around the black hole. (The potentials for this case are easily obtained by turning the ones in Figure 19 upside down.) We then find from (8.6) that

$$V_+ = 0 \text{ at } r = 2M \ , \quad (8.13)$$

and it is clear that some forward-going photons (that must lie above V_+ according to our previous analysis) can have $E < 0$. That is, negative energy (as measured at infinity) photons may exist close to the black hole (for $r < 2M$ in the equatorial plane)! As can be inferred from Figure 19 these negative energy photons can never

escape to infinity, but the fact that they can exist has an interesting consequence.

Let us suppose that a pair of photons, the total energy of which is zero, are created in the region $r_+ < r < 2M$. The positive energy photon can then escape to infinity, while the negative energy one must eventually be swallowed by the hole. The net effect of this would be that rotational energy is carried away from the black hole, and it will slow down. This energy extraction process, that was first suggested by Penrose [17], can be extended to other objects. One can simply assume that a body breaks up into two or more pieces. If one of them is injected into a negative energy orbit the sum of the total energy of the remaining pieces must be greater than the total energy of the original body, since E is a conserved quantity. As in the case of photons, the extra energy is mined from the rotation of the black hole. But however exciting the possibility may seem, the Penrose process is unlikely to play a role in an astrophysical setting.

B. The ergosphere

As we have seen, there is a region close to a rotating black hole ($r < 2M$ in the equatorial plane) where energy becomes 'peculiar'. This is the so-called ergosphere, and since there are many interesting effects (like the Penrose process) associated with it, it is worthwhile to discuss it in more detail.

Let us consider a photon emitted at some r in the equatorial plane ($\theta = \pi/2$) of a Kerr black hole. Assume that the photon is initially moving in the $\pm\varphi$ direction. That is, it is inserted in an orbit that is tangent to a circle of constant r. In this situation it is clear that only dt and $d\varphi$ will be nonzero, and we find from $ds^2 = 0$ that

$$\frac{d\varphi}{dt} = -\frac{g_{t\varphi}}{g_{\varphi\varphi}} \pm \sqrt{\left(\frac{g_{t\varphi}}{g_{\varphi\varphi}}\right)^2 - \frac{g_{tt}}{g_{\varphi\varphi}}} \ . \qquad (8.14)$$

From this we can see that something interesting happens if g_{tt} changes sign. At a point where $g_{tt} = 0$ we have the two solutions

$$\frac{d\varphi}{dt} = -2\frac{g_{t\varphi}}{g_{\varphi\varphi}} \ , \qquad \text{and} \qquad \frac{d\varphi}{dt} = 0 \ . \qquad (8.15)$$

In the Kerr geometry the first case corresponds to a photon moving in the direction of the rotation of the black hole. The second solution, however, indicates that a photon sent "backwards" does not (initially) move at all! The dragging of inertial frames has become so strong that the photon cannot move in the direction opposite to the rotation. Consequently, all particles must rotate with the hole, and no observers can remain at rest (at constant r, θ, φ) in the ergosphere.

As the above example indicates, the boundary of the ergosphere follows from $g_{tt} = 0$. In the Kerr case we find that this corresponds to

$$\Delta - a^2 \sin^2\theta = 0 \ , \qquad (8.16)$$

or

$$r_{\rm ergo} = M \pm \sqrt{M^2 - a^2\cos^2\theta} \ . \qquad (8.17)$$

From this follows that the ergosphere always lies outside the event horizon (even though it touches the horizon at the poles).

C. Teukolsky's equation

We want to extend our study of various scattering scenarios to the Kerr case. To do so, we need to discuss perturbations of the Kerr geometry. It turns out that this problem is considerably more complicated than the Schwarzschild one. For example, the direct derivation of the equations governing perturbations of Kerr spacetimes by considering perturbations of the metric fails. It leads to gauge-dependent, and rather messy, formulations in which one cannot readily separate the variables as in (3.3).

A theoretically attractive alternative is to examine *curvature* perturbations. Using the Newman-Penrose formalism, Teukolsky (1973) derived a master equation governing not only gravitational perturbations (spin weight $s = \pm 2$) but scalar ($s = 0$), two-component neutrino ($s = \pm 1/2$) and electromagnetic ($s = \pm 1$) fields as well. In Boyer-Lindquist coordinates and with the use of the Kinnersley null tetrad, this master evolution equation reads

$$\begin{aligned}
&-\left[\frac{(r^2+a^2)^2}{\Delta} - a^2\sin^2\theta\right]\partial_{tt}\Psi - \frac{4Mar}{\Delta}\partial_{t\phi}\Psi \\
&-2s\left[r - \frac{M(r^2-a^2)}{\Delta} + ia\cos\theta\right]\partial_t\Psi \\
&+\Delta^{-s}\partial_r\left(\Delta^{s+1}\partial_r\Psi\right) + \frac{1}{\sin\theta}\partial_\theta\left(\sin\theta\partial_\theta\Psi\right) \\
&+\left[\frac{1}{\sin^2\theta} - \frac{a^2}{\Delta}\right]\partial_{\phi\phi}\Psi + 2s\left[\frac{a(r-M)}{\Delta} + \frac{i\cos\theta}{\sin^2\theta}\right]\partial_\phi\Psi \\
&-\left(s^2\cot^2\theta - s\right)\Psi = 0 \qquad (8.18)
\end{aligned}$$

The actual meaning of Ψ for various spin-fields is rather complex, so we will only worry about two special cases here. Firstly, for $s = 0$ Ψ represents the scalar field (Φ) itself and in the limit $a \to 0$ we recover the Schwarzschild scalar wave equation. For $s = \pm 2$ the Ψ corresponds to the Weyl curvature scalars Ψ_0 and Ψ_4 that directly represent the gravitational-wave degrees of freedom.

The great breakthrough that followed Teukolsky's derivation of (8.18) was that one could now separate the variables also for Kerr perturbations. For our present purposes it is sufficient to note that this essentially corresponds to assuming that i) the time-dependence of the perturbation is accounted for via Fourier transformation, and ii) there exists a suitable set of angular function that can be used to separate the coordinates r and θ. In the case of scalar perturbations, the angular functions turn out to be standard spheroidal wavefunctions. Knowing

this we assume a representation (for each given integer m)

$$\Phi = \int d\omega\, e^{-i\omega t} \sum_{l=0}^{\infty} R_{lm}(r,\omega) S_{lm}(\theta,\omega) \ , \qquad (8.19)$$

where it should be noted that the angular functions depend explicitly on the frequency ω. That is, they are intrinsically time-dependent functions. After separation of variables, the problem is reduced to a single ordinary differential equation for $R_{lm}(r,\omega)$. This equation can be written as

$$\frac{d^2 R_{lm}}{dr_*^2} + \left[\frac{K^2 + (2am\omega - a^2\omega^2 - E)\Delta}{(r^2+a^2)^2} - \frac{dG}{dr_*} - G^2 \right] R_{lm} = 0 \ , \qquad (8.20)$$

where $K = (r^2+a^2)\omega - am$, $G = r\Delta/(r^2+a^2)^2$, and the tortoise coordinate r_* is defined from $dr_* = (r^2+a^2)/\Delta\, dr$. The variable E is the angular separation constant. In the limiting case $a \to 0$, it reduces to $l(l+1)$, and for nonzero a it can be obtained from a power series in $a\omega$. It should be noted that E is real valued for real frequencies.

D. Quasinormal modes

The physical solution to (8.20) is defined by the asymptotic behaviour (cf. the Schwarzschild result)

$$R_{lm} \sim \begin{cases} e^{-i(\omega - m\,\omega_+)\, r_*} & \text{as } r \to r_+ \ , \\ A_{\rm out} e^{i\omega r_*} + A_{\rm in} e^{-i\omega r_*} & \text{as } r \to +\infty \ . \end{cases} \qquad (8.21)$$

where $\omega_+ \equiv a/2\,M\,r_+$ is the angular velocity of the event horizon.

From this we see that we can define the quasinormal modes of a Kerr black hole in the same way as we did in the spherically symmetric case. Furthermore, these modes can also be calculated using Leaver's continued fraction method. The results can be summarised as follows: Recall that in the non-rotating case the modes occur in complex-frequency pairs ω_q and $-\bar{\omega}_q$ (the bar denotes complex conjugation). This is apparent in Figure 14. As the black hole spins up, each Schwarzschild mode splits into a multiplet of $2l+1$ distinct modes (in analogy with the Zeeman splitting in quantum mechanics). These modes are associated with the various values of m, where $-l \le m \le l$, which determine the modal dependence on the azimuthal angle through $e^{im\varphi}$. As is straightforward to deduce, modes for which Re ω_q and m have the same sign are co-rotating with the black hole. Similarly, modes such that Re ω_q and m have opposite signs are counter-rotating. The effect that rotation has on the mode-frequencies can, to some extent, be deduced from this fact.

Let us first consider the counter-rotating modes: These will appear to be slowed down by inertial frame dragging close to the black hole. Hence, their oscillation frequencies will tend to decrease as $a \to M$. At the same time, numerical calculations show that the damping rate stays almost constant. For the co-rotating modes, the effect is the opposite. Frame-dragging tends to increase the frequencies. Additionally, the modes become much longer lived. The available numerical results for co-rotating modes are well approximated by (cf. [10])

$$\text{Re}\ \omega_0 \approx \frac{1}{M}\left[1 - \frac{63}{100}(1-a/M)^{3/10}\right] \ , \qquad (8.22)$$

and

$$\text{Im}\ \omega_0 = \frac{(1-a/M)^{9/10}}{4M}\left[1 - \frac{63}{100}(1-a/M)^{3/10}\right] \ . \qquad (8.23)$$

From this we can see that the mode becomes undamped in the limit $a = M$. One can actually show (since the case $a = M$ is amenable to analytic methods) that there exists an infinite sequence of real resonant frequencies with a common limiting point in that case. The limiting frequency is $\omega = m/2M$, which we will later show to be the upper limit for so-called super-radiance. That the modes become undamped can be understood from the fact that the angular frequency of an extreme Kerr black hole is $1/2M$. As $a \to M$ the long lived quasinormal modes essentially rotate uniformly with the black hole, and as a consequence they do not radiate strongly.

Provided that the modes of close to extreme rotating black holes will be excited by some realistic astrophysical process, the fact that these modes can be very long-lived would greatly improve the chances for detection with future gravitational-wave detectors. Hence, it is of interest to investigate the excitation of these long lived modes. Recent work has shown that the modes tend to be harder to excite than the short-lived Schwarzschild modes, but that the slowly damped modes nevertheless dominate the emerging signals. An example of this is shown in Figure 20.

E. Superradiant scattering

Given the prescribed asymptotic behaviour (8.21), together with that for the complex conjugate of R_{lm} and the fact that two linearly independent solutions to (8.20) must lead to a constant Wronskian, it is not difficult to show that

$$(1 - m\,\omega_+/\omega)|T|^2 = 1 - |S|^2 \ . \qquad (8.24)$$

where we have introduced the transmission and reflection coefficients as in the Schwarschild case;

$$|T|^2 = \left|\frac{1}{A_{\rm in}}\right|^2 \ , \qquad |S|^2 = \left|\frac{A_{\rm out}}{A_{\rm in}}\right|^2 \ ,$$

From this result, it is evident that the scattered waves are amplified ($|S|^2 > 1$) if

$$\omega < m\,\omega_+ \qquad (8.25)$$

FIG. 20: The response of a near extreme Kerr black hole after a Gaussian scalar wave pulse has impinged upon it. The main features are the same as in the Schwarzschild case (Figure 13), but here the quasinormal mode ringing is much slower damped.

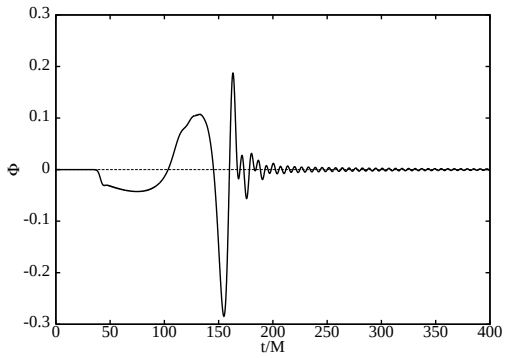

This is known as superradiance and it is the wave-analogue to the Penrose process that we described earlier. Its existence implies that it would in principle be possible to mine a rotating black hole for some of its rotational energy.

In Figure 21, we show a sample of results for the reflection coefficient in the case when $l = m = 2$. These results were obtained by a straightforward integration of (8.20) and subsequent extraction of $\mathcal{R}$. The maximum amplification in this case is a minute 0.2 %. Similar results for electromagnetic waves and gravitational perturbations show that the maximum amplification is 0.3% for scalar waves, 4.4% for electromagnetic waves and as large as 138% for gravitational waves.

Given the results in Figure 21, it is worth pointing out that they agree with standard conclusions regarding the apparent "size" of a rotating black hole as seen by different observers. A rotating black hole will appear larger to a particle moving around it in a retrograde orbit than to a particle in a prograde orbit. This is illustrated by the fact that the unstable circular photon orbit (at $r = 3M$ in the non-rotating case) is located at $r = 4M$ for a retrograde photon, while it lies at $r = M$ for a prograde photon. The results in Figure 21 illustrate the same effect: In our case, we have prograde motion when ω/m is positive and retrograde motion when ω/m is negative. The data in Figure 21 correspond to $m = 2$, and the enhanced reflection for positive frequencies as $a \to M$ has the effect that the black hole "looks smaller" to such waves. Conversely, the slightly decreased reflection for negative frequencies leads to the black hole appearing "larger" as $a \to M$. A sample of results showing this effect is in Table III.

F. Scattering of waves by Kerr black holes

One can analyse the scattering of monochromatic waves by a Kerr black hole in much the same way as we approached the Schwarzschild case. The same is true also for wave fields other than scalar waves. The analysis of electromagnetic and gravitational wave scattering is, in principle, identical to that for scalar waves. However, in the case of gravitational waves an additional complication enters: Gravitational waves come with two different polarisations. This means that the scattering amplitude consists of a sum of their individual contributions, and that the cross section may show features due to interference between these two contributing terms. This effect has not been explored in detail as yet.

Similarly, despite a few studies, the full details of scattering from rotating black holes remain to be understood. Scattering of gravitational waves incident along the axis of symmetry of a Kerr black hole show that the scattering cross section depends in a complicated way on the rotation parameter a. One would essentially expect Kerr

FIG. 21: Reflection coefficient for different values of a in the case $l = m = 2$. Upper panel: As a increases, there is a clearly enhanced reflection of prograde waves ($\omega > 0$ in the figure) while the overall reflection of retrograde waves ($\omega < 0$ in the figure) decreases somewhat. Lower panel: A blow-up of the result for prograde waves unveils a maximum amplification due to superradiance of 0.187%.

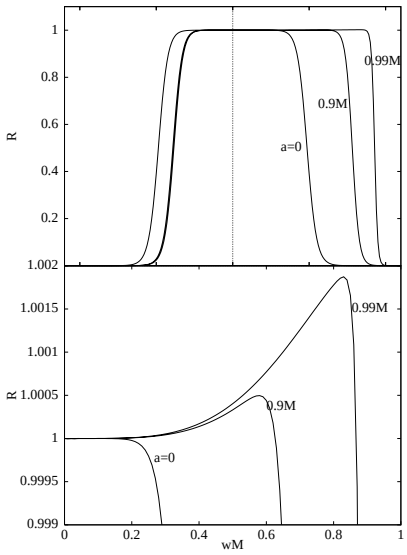

TABLE III: The apparent size b of a Kerr black hole as viewed along the rotation axis. The values are all for $a = 0.9M$ and are estimated from the total absorbtion cross section $\sigma^{\rm abs} \approx \pi b^2$. Positive frequencies co-rotate with the black hole whereas negative ones are counter-rotating. The values should be compared to $b = 5.2M$ for a Schwarzschild black hole.

ωM	-1.5	-0.75	0.75	1.5
$\sigma^{\rm abs}$	$80.3M^2$	$88.7M^2$	$62.5M^2$	$36.5M^2$
b	$5.06M$	$5.31M$	$4.46M$	$3.41M$

scattering to be different because of two effects that do not exist for nonrotating holes: superradiance and the polarization of the incident wave. For incidence along the symmetry axis of a rotating black hole one can have either co- or counter-rotating waves. The two cases lead to quite different results. Although the general features of the corresponding cross sections are similar they show different structure in the backward direction. This possibly arises because of the phase-difference between the two polarisations of gravitational waves. As for superradiance, it has been suggested that it tends to wash out interference minima. Further details can be found in the book by Futterman, Handler and Matzner [19].

Acknowledgments

Figure 16 is from unpublished work by BJ and Antoine Folacci. We would like to thank P. L. Jensen for supplying the original artwork for Figure 1.

[1] P. Schneider, J. Ehlers and E.E. Falco *Gravitational lenses* (Springer Verlag, Berlin, 1993)
[2] K.S. Thorne *Probing black holes and relativistic stars with gravitational waves* in *Black holes and relativistic stars* Ed: R.M. Wald (University of Chicago Press, 1997)
[3] S. Chandrasekhar *The Mathematical Theory of Black Holes* (Clarendon Press, Oxford 1983).
[4] K.W. Ford, and J.A. Wheeler *Ann. Phys.* **7** 259 (1959); *Ann. Phys.* **7** 287 (1959)
[5] Andersson N. and K.-E. Thylwe (1994): *Class. Quantum Grav.* **11**:2991.
[6] C. Darwin *Proc. R. Soc. London A* **249** 180 (1959); *Proc. R. Soc. London A* **263** 39 (1961).
[7] C. DeWitt-Morette and B.L. Nelson, *Phys. Rev. D* **29**, 1663 (1984); R.A. Matzner, C. DeWitt-Morette, B.L. Nelson and T.-R. Zhang, *Phys. Rev. D* **31**, 1869 (1985).
[8] C.V. Vishveshwara *Nature* **227**, 936 (1970)
[9] H.-P. Nollert *Class. Quantum Grav.* **16** R159 (1999)
[10] E.W. Leaver *Proc. R. Soc. London A* **402** 285 (1985).
[11] B.F. Schutz and C.M. Will *Ap. J.* **291** , L33 (1988).
[12] C.J. Goebel *Ap. J.* **172** L95 (1972) .
[13] H.M. Nussenzweig *Diffraction effects in semiclasssical scattering* (Cambridge University Press, 1992)
[14] V.P. Frolov and I.D. Novikov *The physics of black holes* (Kluwer 1998)
[15] S.W. Hawking *Commun. Math. Phys.* **43**, 199 (1975).
[16] J. M. Bardeen, in *Black Holes*, C. DeWitt and B.S. DeWitt eds, (Gordon and Breach, New York, 1973).
[17] R. Penrose *Rel. del Nuovo Cimento* **1** 252 (1969).
[18] S.A. Teukolsky *Ap. J.* **185** 635 (1973).
[19] J.A.H. Futterman, F.A. Handler and R.A. Matzner *Scattering from Black Holes* (Cambridge Univ. Press 1988).